EUV Off-Axis Focussing Using a High Harmonic Source

B. Mills[*a], E. T. F. Rogers[a], J. Grant-Jacob[a], S. L. Stebbings[b], M. Praeger[b], A. M. de Paula[c], C. A. Froud[d], R. T. Chapman[e], T. J. Butcher[a], W. S. Brocklesby[a], J. G. Frey[e]

[a]Optoelectronics Research Center, University of Southampton, UK
*Tel: 023 8059 2610 Email: bem@orc.soton.ac.uk
[b]School of Physics and Astronomy, University of Southampton, UK
[c]Federal University of Minas Gerais, Brazil
[d]Rutherford Appleton Laboratory, UK
[e]School of Chemistry, University of Southampton, UK

Please note this version of the paper may not be exactly as finally published.

ABSTRACT

High Harmonic Generation is an established technique for generating Extreme Ultraviolet radiation. It is a promising technique for both structure and spectroscopic imaging due to both the high flux and coherence of the source, and the existence of multiple absorption edges at the generated wavelengths. To increase the flux, a focussing device can be used. Here we present focussing results for a Mo/Si spherical mirror that has been used in an off-axis arrangement, and give extensive analysis of the resulting astigmatic focus and its consequence on diffractive imaging. The astigmatic beam exists as a vertical and horizontal focus, separated by a circle of least confusion. With the help of a theoretical model we show that the most intense part of the beam is always the second line foci and that the phase at the focus is strongly saddle-shaped. However, this phase distortion cannot explain the significant interference peak splitting that is experimentally observed in our diffraction patterns. Instead we propose that the beam quality is degraded upon reflection from the multilayer mirror and it is this asymmetric phase distortion that causes the diffraction peak splitting.

Keywords: Extreme Ultraviolet, High Harmonic Generation, Off-axis Focusing, Beam Quality, Multilayer Mirror

1. INTRODUCTION

In this section, an outline of the Extreme Ultraviolet (EUV) generation technique and the experimental setup used in this investigation is presented.

1.1 High Harmonic Generation

High Harmonic Generation (HHG) is a well established technique for generating EUV light using an ultrafast laser [1-3]. Typically, an ultrafast laser is focussed into a region of low pressure gas and EUV photons are generated with an efficiency of ~10^{-6}. The intense electric field of the laser can ionise an outer electron from a gas atom, and then accelerate it away from the ion. When the electric field changes direction approximately half an optical cycle later, the electron may return to its parent ion. It is the combination of the kinetic energy gained by the electron and the ionisation potential that can be used to generate an EUV photon. As the EUV is generated twice per optical cycle, the measured spectrum consists of odd harmonics of the fundamental laser wavelength. If argon gas is used as the generation medium, typically, the 23rd to 33rd harmonics (35 to 24 nm, 36 to 51 eV) are generated with a spectral width of ~1 nm, with an intensity of ~10^{11} photons per second per harmonic [4], although shorter wavelengths are observed using other gases and configurations [5]. The intense EUV beam is strongly coherent [6] and hence there is great interest in using HHG for both nanoscale structure determination [7-8] and spectroscopic measurements [9].

To increase the flux, the EUV beam can be focussed. Typically, a multilayer mirror is used. Here there are two options: a spherical mirror used in an off-axis arrangement, or an off-axis paraboloidal mirror. Spherical mirrors are significantly easier to produce than off-axis paraboloidal mirrors. However, due to the nature of the reflection geometry, spherical mirrors must be used at a non-zero incident angle, and the result of this is an astigmatic focus. In this paper we discuss the properties of this focus with the aim of understanding the aberration and finding the optimal focussing geometry for both nanoscale imaging and spectroscopic measurements.

1.2 Experimental Setup

For the results presented here, the 40fs output pulses from an 800 nm, 1 kHz repetition rate, 1.5 Watt laser system were focussed using a concave mirror with radius of curvature (ROC) of 1000 mm, into a 150 μm diameter hollow glass capillary of length 5 cm, with an argon pressure of 70 mbar. By using appropriate coupling techniques, transmission percentages of ~60% are achieved. As the EUV and fundamental laser propagate collinearly, they are separated using transmission through a 200 nm thick aluminium foil, which transmits ~10^{-2} of the EUV whilst attenuating the fundamental laser by ~10^{8}. Inside the main vacuum chamber, a Mo/Si multilayer spherical concave mirror (ROC = 500 mm) is used at an incident angle of ~10 degrees to focus the EUV beam down to a spot size (w_0, defined as the $1/e^2$ intensity beam radius [10]) of ~30 μm. The spatial intensity profile is recorded using a water-cooled EUV CCD camera (Andor, 1024x1024 13 μm pixels), which is moved in steps of 1 mm through the focus, with typical integration times of 100 ms. Figure 1 shows this experimental setup. The mirror angle is the minimum possible for our experimental geometry and is limited by the width of the CCD camera.

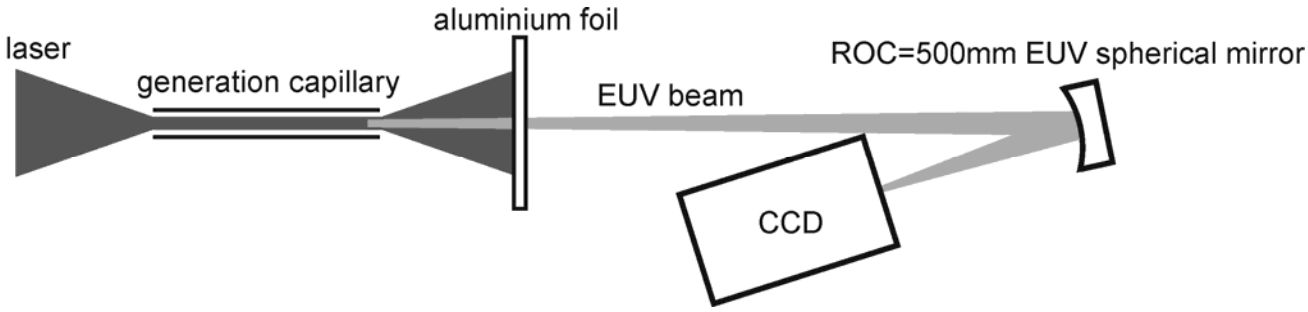

Fig. 1. Schematic of the experimental setup showing: the generation capillary which contains 70 mbar of argon, transmission through 200 nm of aluminium to separate the EUV from the laser, and the spherical mirror focussing arrangement inside the chamber. The minimum angle of the spherical mirror is directly limited by the width of the CCD. For diffraction experiments, the CCD is moved away from the focus and replaced by a diffraction sample.

2. THEORETICAL MODEL

In this section the theoretical framework for analysing an astigmatic beam is presented. By modelling the experimental results, this framework enables parameters such as the EUV beam quality to be accurately determined and shows how changing the parameters will affect the spot size and EUV intensity and phase at the focus.

2.1 Astigmatism as a result of off-axis focussing

A spherical mirror at normal incidence (zero angle) has the same ROC for both the horizontal (x) and vertical (y) axes. However, for a non-zero angle, both the x and y ROC change. The consequence is distinct vertical and horizontal line foci, which are separated by a circle of least confusion (CLC) that is present at the defined mirror focal length. It is important to realise that although the intensity profile at the CLC is circular, the phase is not flat. This is a simple consequence of different values for the x and y ROC. Treating the x and y axes separately at the CLC, one axis is diverging and one is converging and therefore the phase at this position is saddle-shaped. This effect can be quantified using the following model.

2.2 Beam propagation using ABCD matrices

To understand the beam intensity and phase through the focus, a 3D model has been constructed. The assumptions are that the propagation angle does not deviate from a small angle, and that the beam is monochromatic. Although the wavelengths in the generated beam have a spectral bandwidth ($\lambda/\Delta\lambda$) of roughly two, the narrower band of wavelengths that are focused by the mirror have a value of greater than ten, and hence can be treated as a monochromatic source. This theoretical approach requires the laser to exist in the lowest order mode. However, the theory can be adapted to higher order propagation modes by introducing the M^2 beam quality parameter, which quantifies how much faster the modelled beam diverges when compared to a Gaussian beam.

For this analysis, the complex beam parameter q is constructed, as defined in equation 1, where λ is the wavelength, ω is the beam spot size, and R is the radius of curvature. The complex beam parameter therefore includes local information on the beam size and the degree of convergence or divergence.

$$\frac{1}{q} = -i\frac{\lambda}{\pi w^2} + \frac{1}{R} \tag{1}$$

The complex beam parameter after an optical element (q') can be related to the parameter immediately before the element (q) using equation 2, using the elements of the ABCD matrix for the element.

$$q' = \frac{Aq + B}{Cq + D} \tag{2}$$

The system to be modelled here, starting from the point of generation inside the capillary, consists of propagation through free space, reflection from an spherical mirror positioned off-axis, and propagation through free space. The spherical mirror profile is modelled as a parabolic surface, as the spherical aberration in this case is negligible. However, the astigmatism is non-negligible, and hence this theoretical model describes the focussing ability of a mirror with a parabolic profile which is arranged off-axis. This is equivalent to the experimental setup shown in figure 1. As mentioned earlier, the ROC imposed on the beam by the mirror is different for the x and y axes. Equations 3 and 4 show the form of the two system matrices for the x and y axes,

$$\begin{pmatrix} A & B \\ C & D \end{pmatrix}_x = \begin{pmatrix} 1 & L \\ 0 & 1 \end{pmatrix} \begin{pmatrix} 1 & 0 \\ -2/R_x & 1 \end{pmatrix} \begin{pmatrix} 1 & z \\ 0 & 1 \end{pmatrix} \tag{3}$$

$$\begin{pmatrix} A & B \\ C & D \end{pmatrix}_y = \begin{pmatrix} 1 & L \\ 0 & 1 \end{pmatrix} \begin{pmatrix} 1 & 0 \\ -2/R_y & 1 \end{pmatrix} \begin{pmatrix} 1 & z \\ 0 & 1 \end{pmatrix} \tag{4}$$

where $R_x = R/\cos(\theta)$ and $R_y = R\cos(\theta)$. L is the fixed distance between the generation capillary and the mirror, θ is the angle of the mirror, and z is the distance from the mirror to a position through the focus, which in this case we want to vary as this provides us with the complex beam parameter at any position through the focus. These calculations are for a mirror that reflects light back at the same height but different yaw angle, i.e. a mirror that has been rotated about a vertical axis.

3. EXPERIMENTAL RESULTS

In this section results are presented that show the intensity profile of the EUV beam measured using an EUV CCD camera, in steps of 1 mm through the focus. From this data, all necessary parameters can be accurately extracted. Section 3.1 discusses these beam parameters and how they are determined. Of particular interest is the beam quality parameter (the M^2 value) which is shown to be increased upon reflection from the EUV mirror. Section 3.2 shows how the theoretical model can be used to optimise the focussing arrangement for both intensity and spot size. Section 3.3 maps the theoretical phase onto the experimentally observed intensity profiles through the focus, showing that the phase shift is large but symmetric, and therefore the phase variation cannot explain the experimentally observed diffraction peak splitting. Section 3.4 investigates the effect of large-scale surface modulations on the surface of the EUV mirror and considers whether this effect can explain the apparent increase in the beam quality parameter. The effect of sampling a distorted intensity profile using resolution that is low relative to the size of the focus is an important consideration here. Finally, the intensity and phase profile that is predicted by a modulated mirror surface is shown to produce a diffraction pattern that has interference peaks which exhibit splitting. This theoretical result shows excellent qualitative agreement with experimentally observed diffraction results using the focussing arrangement that has been simulated, and therefore gives further evidence that the mirror surface figure is affecting the quality of the EUV beam.

3.1 Beam quality calculation

In this section we show how the mirror angle, beam M^2, and the spot size inside the capillary where the EUV is generated can be determined from the intensity profile of the EUV beam through the astigmatic focus.

Figure 2 shows the experimentally measured spot size for the horizontal (x) and vertical (+) axes. The line foci correspond to points of inflexion in the horizontal and vertical axes curves. The vertical focus exists at ~0.247 m, the CLC ~0.250 m, and the horizontal focus ~0.254 m. The best fit theoretical curves (solid lines) are calculated by utilising the ABCD matrix model discussed in Section 2.2. This approach is more accurate than simply fitting the data points for the individual axes to a Gaussian beam propagation equation as the angle of the mirror changes its apparent curvature for each axis, and hence all the parameters are to some extent interdependent. Firstly, the mirror angle affects the relative separation of the line foci and can therefore be easily determined. It does however have a secondary effect on the ROC for the two axes and hence must be determined first. Once the angle has been determined, both the beam M^2 and the focussed spot size (w_0) can be uniquely determined as increasing the M^2 increases the beam size at both the focus and the far-field, whilst increasing the focussed spot size directly decreases the beam size in the far-field. As the generation and focussing geometries and distances are known, the calculation of these parameters enables the size of the EUV focus at

the point of generation inside the capillary to be determined. This corresponds to the spatial properties of the EUV when it is generated, and therefore provides useful information. The mirror angle and capillary spot size are determined to be 9.55 ± 0.1 degrees (directly observed by eye to be 10 degrees) and 65 ± 5 μm. The M^2 in the horizontal and vertical axes are 14.0 ± 1 and 16.6 ± 1.

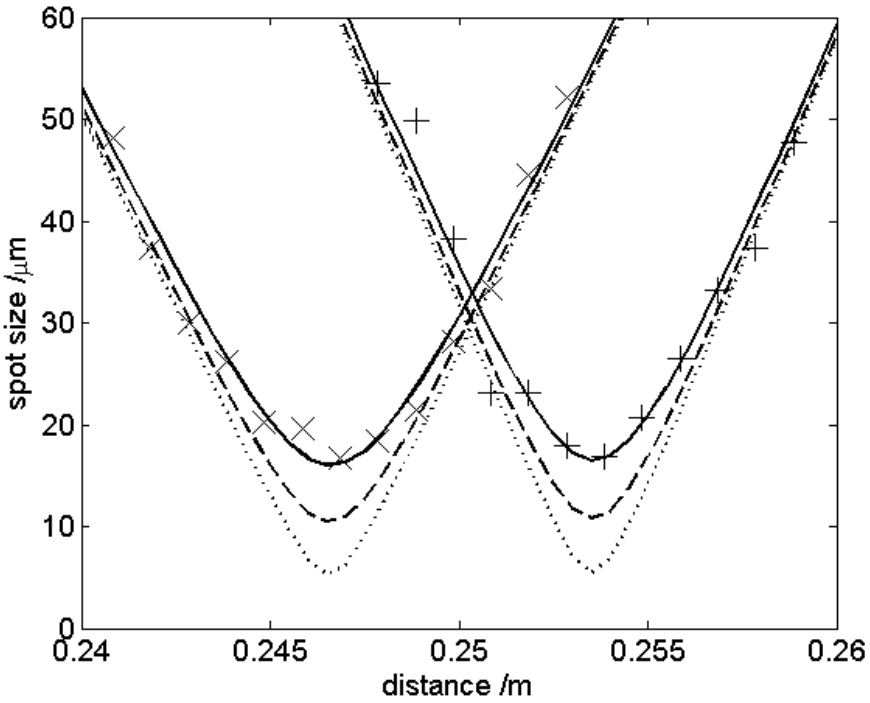

Fig. 2. Experimentally observed horizontal (x) and vertical (+) spot sizes through the astigmatic focus, where the solid lines correspond to a mirror angle of 9.55 degrees and M^2 values of 14 and 16.1 for the two beam axes. Also showing the effect on the focussed spot size if the M^2 increase by the mirror was only to 10 (dashed line) and 5 (dotted line). The figure shows that a reduced M^2 will not significantly decrease the spot size at the CLC, and therefore instead the astigmatism is the limiting factor.

The analysis above implies that the EUV at the point of generation inside the capillary has a radius of 65 ± 5 μm. This is unlikely for the following reason. The EUV beam is generated only where the fundamental laser light is sufficiently intense. As the boundary conditions for an electric field inside a dielectric capillary result in zero intensity at the edges *and* the high-order capillary modes are lossy and therefore do not exist at the EUV generation point towards the end of the capillary, the EUV beam must be significantly smaller than 65 um. Radial-phase matching calculations have shown that for an identical setup, the theoretical XUV radius is ~15 μm [11].

Using the ABCD matrix framework and working backwards from the data in figure 2, the size of the EUV beam at the position of the multilayer mirror can be calculated. Using this and the calculated generated spot size of 15 μm gives an M^2 value of ~3, where the sensitivity on the generated spot size is such that 15 ± 5 μm implies a generated EUV M^2 of 3 ± 1. The generated M^2 is therefore different to the M^2 value measured at the focus. The likely reason here is that although the surface roughness of the multilayer mirror is sub nanometer, the surface figure (quoted as less than λ/10 at 663 nm) of the mirror is such that a variable phase shift is imparted upon the EUV beam, causing the beam quality to be degraded. A surface figure of λ/10 at 633 nm corresponds to a value of ~2λ at 30 nm, and therefore a significant phase shift could occur across the EUV beam should the mirror surface deviate at the point of illumination. A model used to quantify this proposition is presented in section 3.4. However, as shown in figure 2, if the proposed increase in the M^2 was reduced to 10 or 5 instead of ~15, the spot size at the CLC would only decrease in size by a few microns. Instead, the astigmatism is the limiting factor for the spot size. The relationship between the spot size and the mirror angle is discussed further in the next section.

3.2 Astigmatic intensity profile through the focus

The theoretical model described in section 2 has been adapted to calculate the spatial intensity profile at the resolution of the EUV CCD. Figure 3 shows a-c) the experimentally observed spatial intensity profile at the two line foci and the CLC and the theoretical predictions d-f) corresponding to parameter values extracted from fig. 2. In both cases the pixel size is 13 μm. The theoretically predicted profiles show strong agreement with the experimentally observed results. However, they are not identical for two reasons. Firstly, the experimentally recorded intensity profiles are not centered over a single pixel. This can explain the difference in the relative intensities of the central pixels. The second reason is due to the

limitation of describing a complex spatial profile by using a single scalar quantity (the M^2 value). Whilst the width of the experimental beam as it propagates has been successfully modelled, the M^2 value does not contain information on the actual spatial profile. Instead the spatial intensity profile is modelled as a Gaussian which diverges by a factor defined by the beam quality parameter. The cause of the degraded intensity profile is explored further in section 3.4, where the effect of a modulated mirror surface is simulated.

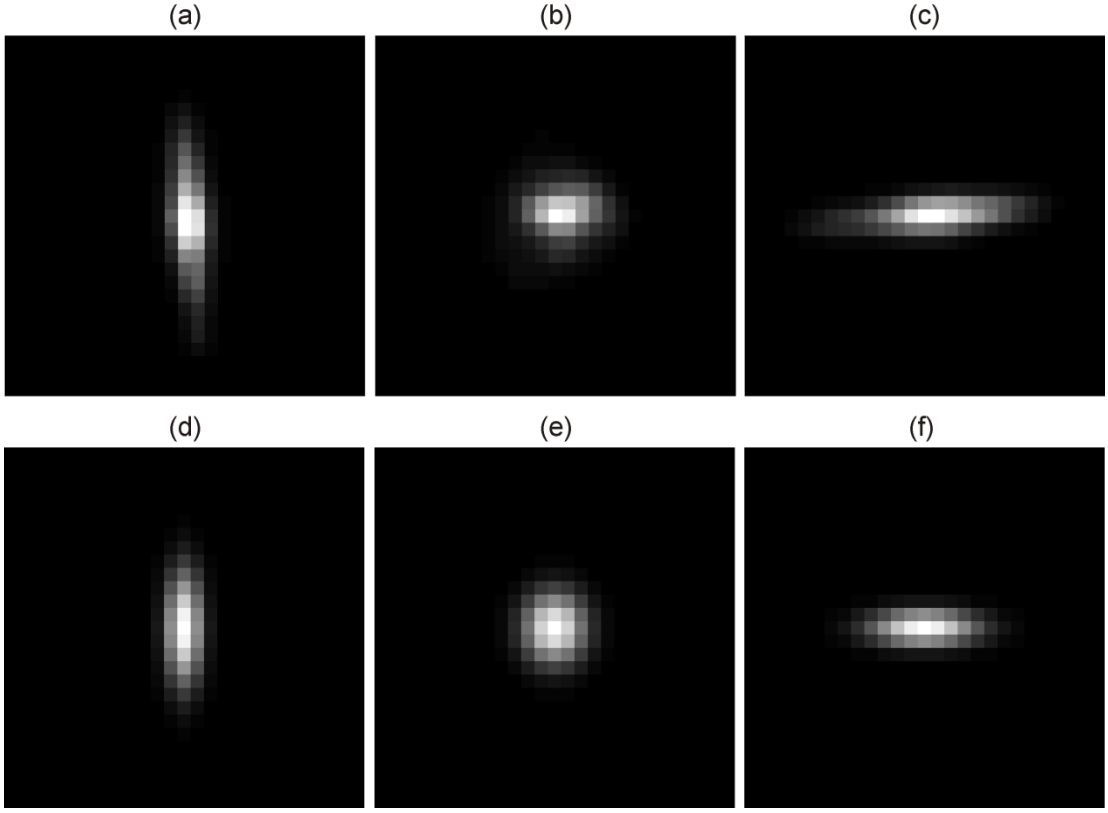

Fig. 3. Experimental a-c) and theoretical d-f) intensity profiles at the horizontal and vertical line foci, along with the intensity profile at the CLC, using the parameters determined from figure 2, showing excellent agreement. Differences are caused by experimental data that is not centralised on a single pixel, and the limitation of the scalar M^2 parameter to quantify a complex spatial beam profile. In all cases, the pixels are 13 μm.

Figure 4 shows the experimental (circles) and theoretical predictions (lines) for the peak pixel intensity through the focus. The theoretical data, corresponding to a 9.55 degree mirror angle and the experimentally determined M^2 values, is shown as the solid line and normalised to the experimental data by making the most intense data points equivalent. The most intense data point for both experiment and theory is the horizontal line foci, and therefore if the peak intensity is to be maximised the sample should be positioned at the horizontal line focus, instead of the CLC. Also shown is the effect on the peak intensity at the CLC if the mirror angle was reduced to 5 degrees (dashed line) and 0 degrees (dotted line), illustrating that the peak intensity at the focus would be almost doubled if the mirror angle was reduced from 9.55 to 5 degrees, whilst further increases in intensity are smaller, and hence a mirror angle of less than 5 degrees is critical for maximising the peak intensity.

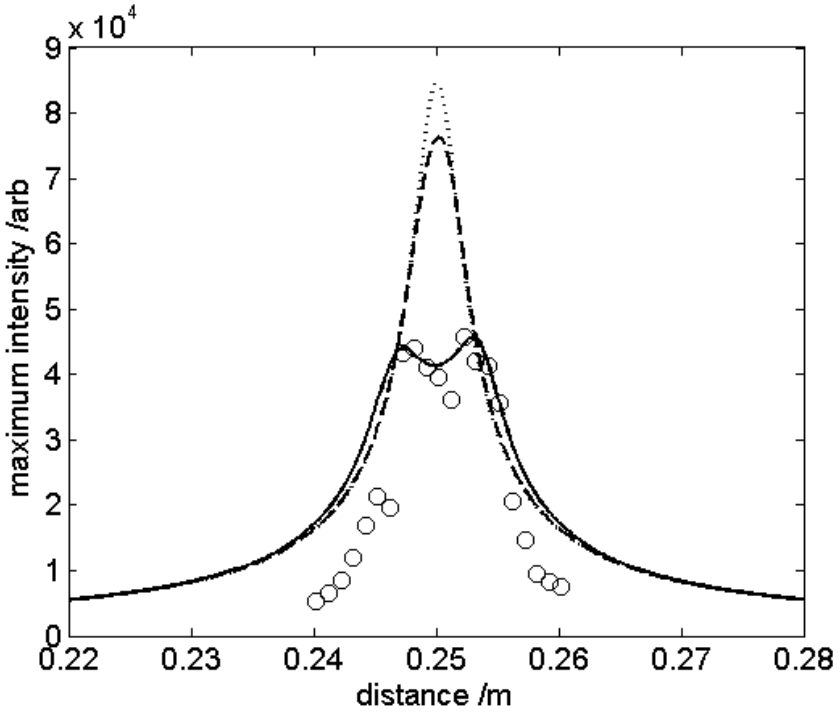

Fig. 4. Peak pixel intensity through the focus for experimental data (o) and the theoretical prediction (solid line) showing that the most intense part of the beam is the horizontal line focus rather than the CLC. Also shown is the effect on the peak intensity by reducing the mirror angle from 9.55 degrees to 5 degrees (dashed line) and 0 degrees (dotted line) illustrating that the peak intensity would be almost doubled if the mirror angle was reduced to 5 degrees, and hence that an angle less than 5 degrees is critical for maximising the focussed intensity.

Figure 4 indirectly shows that the spot size at the CLC will be reduced if the mirror angle is reduced, as the peak intensity is shown to increase. However, the spot size is a function of both the mirror angle and the mirror ROC. To increase the focussed intensity the mirror angle should be reduced and the mirror ROC decreased. However, as shown in figure 5, the relationship is nonlinear. For a mirror angle of 0 degrees, the spot size is generally proportional to the mirror ROC. However, for a fixed mirror angle of 10 degrees, a shorter focal length mirror will only slightly decrease the spot size. Therefore, for mirror angles greater than 10 degrees, the most significant improvement in peak intensity will result from a decreased angle. Due to the nonlinear relationship, the combination of a longer mirror focal length and the possible corresponding smaller mirror angle can actually result in a tighter focus and a higher intensity. Therefore, a smaller ROC will not always increase the intensity at the beam focus.

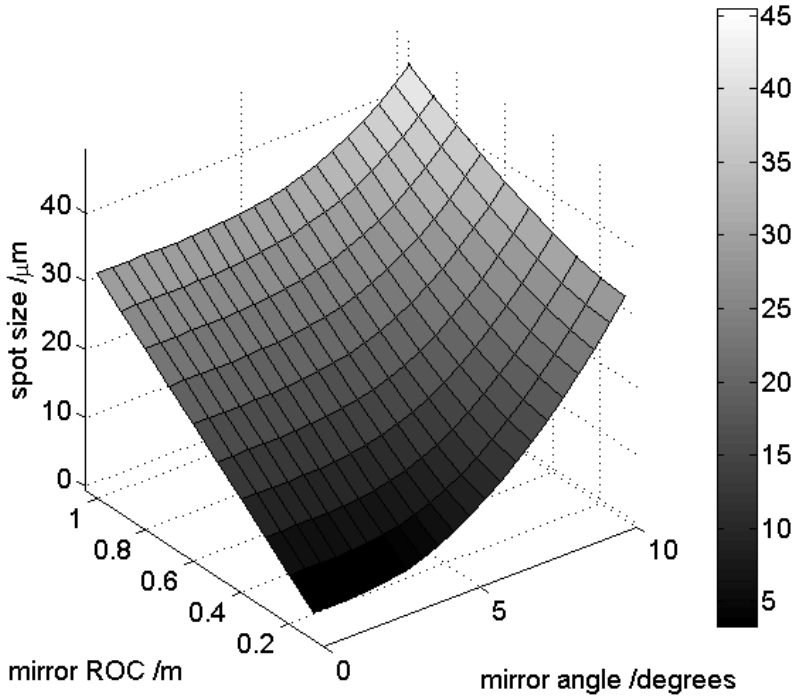

Fig. 5. Focussed spot size as a function of mirror ROC and mirror angle, for the experimentally determined parameters. For an angle near to zero degrees, the spot size and mirror ROC are generally proportional. For an angle of 10 degrees, diminishing returns exist for mirrors with a shorter ROC. Due to the nonlinear relationship, increasing the mirror ROC if it enables a smaller mirror angle can actually reduce the focus spot size and hence increase the intensity.

3.3 Astigmatic phase profile through the focus

The beam curvature imposed on the beam by the mirror is such that the horizontal and vertical foci do not coincide. Therefore, at the CLC, one axis is converging and one is diverging. Hence the phase at this position is saddle-shaped. Shown in figure 6 is the theoretically predicted phase through the focus, overlaid onto the experimentally observed intensity profiles. In order to highlight the phase modulations, the figure shows cos(φ), where φ is the phase angle across the beam. For an angle of 9.55 degrees, a spherical mirror with focal length 250 mm will have a significant phase variation across the beam. As discussed earlier, the phase at the CLC is saddle-shaped. For the line foci, the phase is flat in one axis and curved in the other. Although the phase variation is large for all positions through the focus, the variation is symmetrical and hence cannot produce the experimentally observed diffraction peak splitting, as the phase variation must have some asymmetry for this result. This principle is discussed further in section 3.4. Although the astigmatic phase will not produce split interference peaks, it will produce a different diffraction pattern to a similar intensity profile with a flat phase and hence is a consideration when using a spherical mirror in an off-axis arrangement for diffractive imaging.

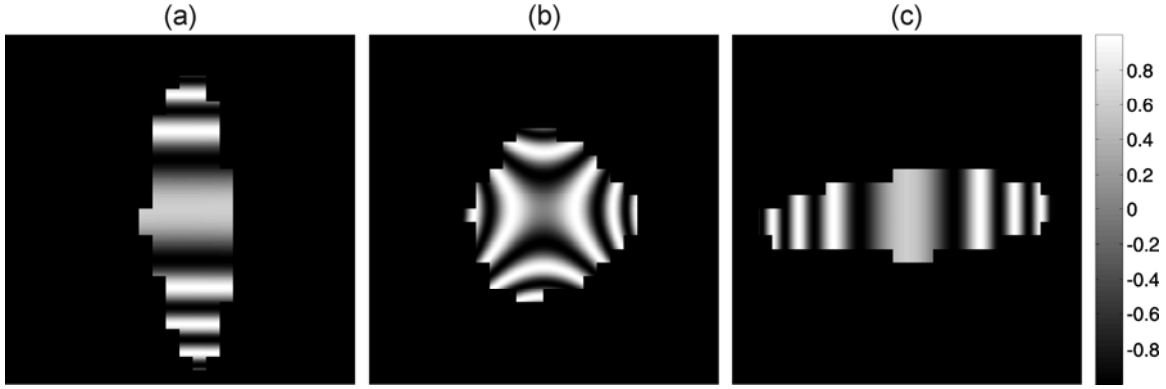

Fig. 6. Theoretical phase, displayed in the form cos(φ) in order to illustrate the phase modulations, mapped onto experimentally observed intensity profiles (as shown in figure 3), for the a) vertical focus, b) CLC and c) horizontal focus. Significant phase variations are predicted through the astigmatic focus. It is important to note that whilst the phase variation will affect diffractive imaging results when compared to a flat phase, the symmetric phase distortion presented here cannot cause the experimentally observed diffraction peak splitting.

3.4 Effect of mirror surface figure

In this section, we give preliminary results from a model that has been used to simulate the EUV mirror surface, and its effect on the quality of the focussed beam. Although the mirror has an extremely low surface roughness, the surface figure (corresponding to long-scale deviations from a perfect spherical profile) is defined as < λ/10 at 633 nm. Although this is suitable for visible radiation, EUV wavelengths (in this case ~30 nm) can require a much higher performance. As discussed in section 3.1, the likely cause of the increase of the beam M^2 is a deviation from a perfect mirror profile. However, it is important to realise that both the surface figure value *and* the correlation length of the deviations must be known in order to accurately quantify the effect of reflection from a mirror. In the results presented here, the latter is not known, and hence instead the problem is approached differently. Given that we observe an increase of the beam M^2, and observe diffraction peak splitting, the work presented here attempts to quantify the mirror surface that would result in this observation. Future work will include optical interferometric results of the mirror surface, which will help to further quantify this model.

The deviation from a perfect spherical surface in nanometers, shown in figure 7a), is simulated by summing 1000 Gaussian distributions with radius ~1 mm, and randomly positioned on the mirror. They have an equal chance of being positive or negative. The height of each Gaussian is randomly determined each time using the uniform distribution with range 0 to 4 nm. The central ~2 mm part of the mirror, shown in fig. 7b), represents the deviation for an area approximately equal to the incident EUV beam.

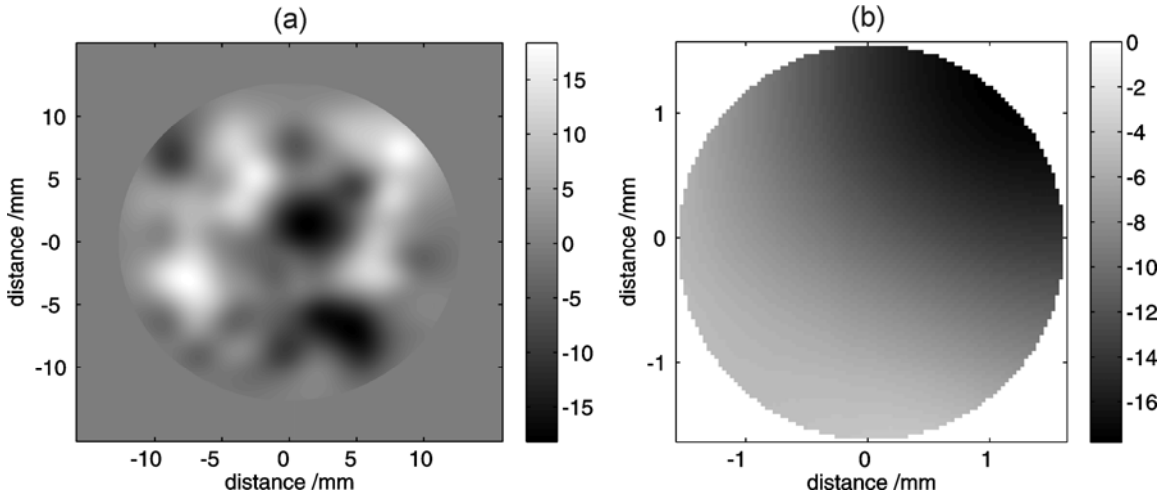

Fig. 7. Simulated deviation from a perfect spherical profile constructed by the combination of 1000 Gaussians with random heights up to 4 nm, with radius of 1 mm for the a) entire mirror surface, and b) mirror surface illuminated by the EUV beam.

By assuming that the incident EUV beam is has a perfect Gaussian intensity profile and a flat phase, the perturbation to the phase can be calculated by taking into account the varying pathlength for each part of the beam. This result is Fourier Transformed to give the intensity and phase of the EUV beam at the mirror focus. The effect of the astigmatic focus is ignored in order to understand the different effect of the two aberrations. Figure 8 shows the simulated a) intensity profile and b) phase profile at the focus, and c) the effect of 'binning' the pixels into a resolution that is similar to the experimental data. The intensity profile in a) is surprisingly asymmetric, and is a direct result of the phase shift corresponding to the surface in figure 7b). However, when figure 8a) is sampled at a resolution equivalent to the CCD, as shown in c), the intensity profile appears considerably more symmetric. This shows qualitative agreement with the experimentally observed intensity profile in figure 2b), showing that this model does not contradict experimental observations of the apparent symmetry of the EUV spatial intensity profile at the focus. This therefore implies that the spatial beam quality may be significantly worse than implied by the experimental data, due to the low resolution of the sampling.

The phase, shown in figure 8b) also exhibits asymmetry, as oppose to the astigmatic phase which possesses rotational symmetry. Simulations show that the effect using the astigmatic intensity and phase for diffraction experiments results in little change when compared to a beam with a flat phase. However, as discussed in more detail later, the asymmetric phase that results from a modulated mirror surface considerably affects the diffraction images, and can successfully explain the experimentally observed interference peak splitting when diffracting from a hexagonal array of 196 nm diameter polystyrene spheres.

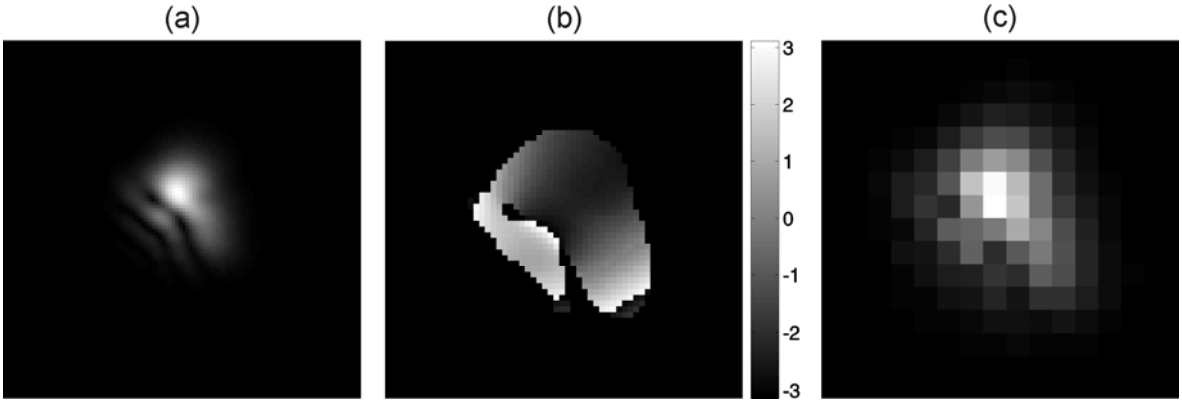

Fig. 8. The theoretical a) intensity and b) phase profiles at the focus, given the mirror surface in figure 7b) showing the predicted asymmetry in the beam profile at the focus. Part c) illustrates the effect of 'binning' the intensity profile onto pixel sizes that are equivalent to the EUV CCD used in this investigation, showing that a non-circular beam profile can appear approximately circular when the sampling resolution is reduced.

The M^2 which corresponds to the intensity and phase in figure 8 has been calculated using the Angular Spectrum Method [12]. Given an arbitrary complex beam, the complex beam corresponding to any propagation distance can be directly calculated. By calculating the profile at ten positions, the beam M^2 for both the horizontal and vertical axes has been determined. For the simulated beam in figure 8, the values 2.2 and 2.5 were calculated. The simulated surface in figure 7b) has therefore increased the beam M^2 by a factor of 2.5, clearly showing that a modulated mirror that deviates from a spherical profile by less than 20 nm over a 1-inch optic can significantly deteriorate a 30 nm EUV beam. This effect is observed experimentally. As shown in section 3.1, the EUV beam quality was observed to be degraded by a factor of ~5. In addition, the simulated beam quality in the horizontal and vertical axes is different, an effect also observed experimentally. This simulation analysis has been repeated for the aluminium foil (see figure 1) using data extracted from scanning electron microscopy and optical microscopy techniques, and shows that the effect of the aluminium foil is near to negligible, with M^2 increases always less than 10% and therefore significantly smaller than the effect of the mirror.

Although the degraded intensity profile is an important consideration, the phase profile at the focus is of paramount importance due to the effect on subsequent diffractive imaging. By moving the CCD from the focus (see figure 1) and replacing it with a periodic sample, the effect of the degraded phase can be illustrated. The sample, a single-layer hexagonal array of 196 nm diameter polystyrene spheres supported on a 50 nm thick silicon nitride substrate, has been discussed elsewhere [mills08]. This sample has also been simulated, by creating a hexagonal array of circles. The theoretical diffraction pattern is therefore the Fourier Transform of the product of the simulated sample and the simulated beam profile from figure 8. Figure 9a) shows the simulated diffraction pattern using the degraded intensity with a flat phase. The hexagonal structure which results from the hexagonal lattice on the sample is clearly shown. Although there is some elongation of the interference peaks, no significant splitting is observed. Figure 9b) shows the simulated diffraction pattern for both the degraded intensity and phase. This result clearly shows the effect of an asymmetric phase on a diffraction pattern. The interference peaks show significant splitting and importantly the splitting does not possess any symmetry.

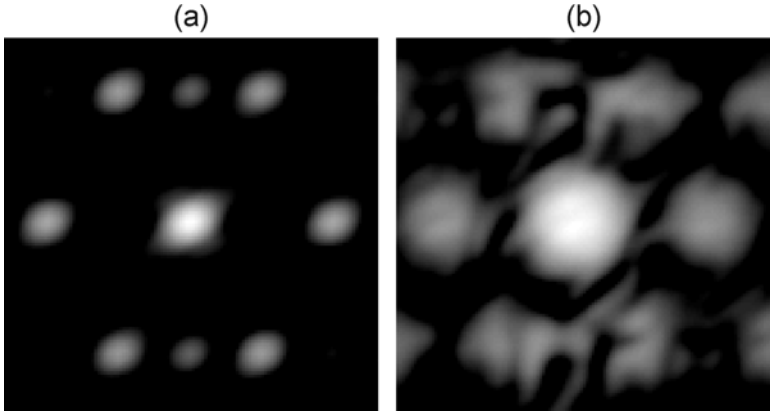

Fig. 9. Simulated diffraction pattern from a hexagonal array of circles when using a) the simulated intensity and a flat phase, and b) both the simulated intensity and phase. The image corresponding to the flat phase does not exhibit splitting of the diffraction peaks, whereas the image corresponding to the degraded phase clearly shows splitting, and also possesses no symmetry.

Figure 10 shows the experimentally observed result. Before a comparison is made there are two important considerations. Firstly, the experimental diffraction peaks are smaller simply as a result of scaling in the Fourier Transform, which was taken advantage of to improve the resolution of the theoretical analysis. Secondly, the experimental result consists of multiple wavelengths, and hence the diffraction peaks are repeated for different angles. Figure 10a) shows the experimental equivalent to the results in figure 9, while parts b) and c) show two of the experimental diffraction peaks in more detail. Although the interference peaks correspond to multiple wavelengths in the axial direction, there is significant splitting. The splitting is unique for each of the interference peaks, and therefore excellent qualitative agreement is demonstrated with the theoretical results in figure 9. This analysis shows that an asymmetric phase at the EUV focus is required to explain the experimentally observed interference peak splitting. However, as it has been shown that the phase distortion resulting from the astigmatic focus cannot produce this effect, there must be another factor introducing additional phase distortions. This section shows that this effect can be explained by the presence of nanometer sized modulations over large distances in the mirror surface, and therefore shows that the mirror surface figure is an extremely important consideration for EUV optics when diffractive imaging is investigated.

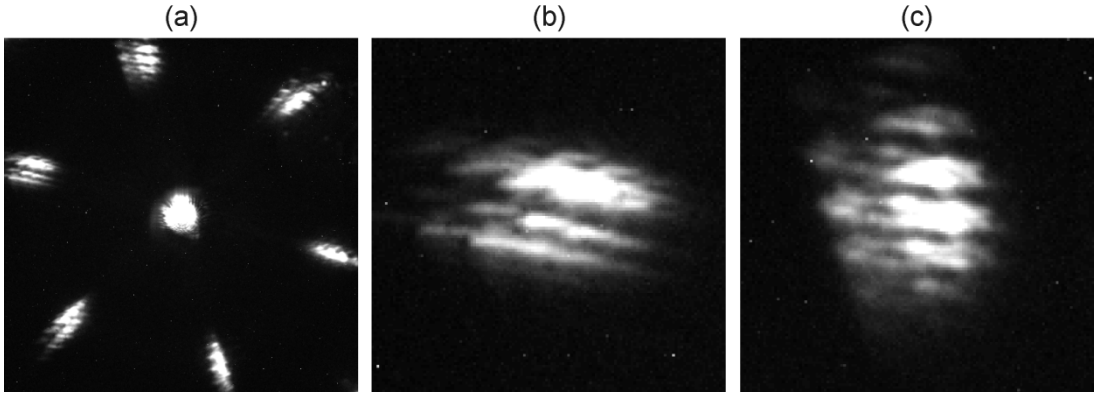

Fig. 10. Experimentally observed diffraction pattern from a single-layer hexagonal array of 196 nm diameter polystyrene spheres, showing a) whole diffraction image, b) left interference peak and c) top interference peak showing significant splitting. The diffraction pattern corresponds to multiple wavelengths (separated in the axial direction) but clearly showing that the observed interference peak splitting in the radial direction can be explained by an asymmetric phase at the focus, a result of modulated mirror surface.

4. CONCLUSION

4.1 Summary

Presented here is an extensive analysis of an astigmatic extreme ultraviolet (EUV) beam, produced when a spherical mirror is used in an off-axis arrangement. By using an experimentally verified 3D model, the balance between the experimental parameters required for an optimal focus has been determined, and hence a quantified comparison can be made with an off-axis paraboloidal mirror. As the focussed spot size is a nonlinear function of the mirror angle and mirror radius of curvature (ROC), increasing the ROC if it allows a smaller mirror angle can actually decrease the spot size and hence increase the peak intensity. However, in order to minimise the phase distortion and maximise the focussed intensity, the mirror angle should be less than 5 degrees. The most intense position through the focus was shown experimental and theoretically to always be the second line focus and not the circle of least confusion. The theoretical model has also enabled a calculation of the EUV beam M^2, at 14.0 ± 1 and 16.6 ± 1 for the horizontal and vertical axes, and has shown that the beam M^2 has been increased upon reflection from the EUV mirror.

The cause of the increase in the beam M^2 is proposed to be the non-zero surface figure parameter for the EUV mirror. This effect has been indirectly investigated by calculating the phase perturbation imparted on an EUV beam upon reflection from a mirror that deviates from a perfect spherical profile. Using this phase perturbation, the theoretical intensity and phase at the EUV focus was calculated and was shown to be degraded in a way that has been observed experimentally. Most importantly however, the simulated beam profile was shown to have a significant effect on the diffraction pattern from a periodic structure. Instead of distinct interference peaks, the interference peaks were found show significant splitting. This effect is observed experimentally and therefore shows that the surface figure of an EUV optic is of critical importance when both focussing and using the focussed source for diffraction imaging.

REFERENCES

[1] Paul, P. M., Toma, E. S., Breger, P., Mullot, G., Auge, F., Balcou, Ph., Muller, H. G., and Agostini, P., H. "Observation of a Train of Attosecond Pulses from High Harmonic Generation", Science, 292, 1689 (2001).

[2] Bartels, R., Backus, S., Zeek, E., Misoguti, L., Vdovin, G., Christov, I. P., Murnane, M. M., and Kapteyne, H. C., "Shaped-pulse optimization of coherent emission of high-harmonic soft x-rays", Nature, 406, 164 (2000).

[3] Lewenstein, M., Salieres, P., and L'Huillier, A., "Phase of the atomic polarization in high-order harmonic generation", Phys. Rev. A, 52(6), 4747 (1995).

[4] Froud, C. A., Rogers, E. T. F., Praeger, M., de Paula, A. M., Hanna, D. C., Baumberg, J. J., Brocklesby, W. S., and Frey, J. G., "Soft-x-ray wavelength shift induced by ionization effects in a capillary", Optics Letters, 31(3), 373 (2006).

[5] Gibson, E. A., Paul, A., Wagner, N., Tobey, R., Gaudiosi, D., Backus, S., Christov, I. P., Aquila, A., Gullickson, E. M., Attwood, D. T., Murnane, M, M., and Kapteyne, H. C., "Coherent Soft X-ray Generation in the Water Window with Quasi-Phase Matching", Science, 302, 95 (2003).

[6] Bartels, R. A., Paul, A., Green, H., Kapteyne, H, C., Murnane, M. M., Backus, S., Christov, I. P., Liu, Y., Attwood, D., and Jacobsen, C., "Generation of Spatially Coherent Light at Extreme Ultraviolet Wavelengths", Science, 297, 376 (2002).

[7] Sandberg, R. L., Paul, A., Raymondson, D, A., Hadrich, S., Gaudiosi, D. M., Holtsnider, J., Tobey, R. I., Cohen, O., Murnane, M, M., and Kapteyne, H, C., "Lensless diffractive imaging using tabletop coherent high-harmonic soft-x-ray beams", Phys. Rev. Letters, 99, 098103 (2007).

[8] Sandberg, R. L., Song, C., Wachulak, P. W., Raymondson, D, A., Paul, A., Amirbekian, B., Lee, E., Sakdinawat, A, E., La-O-Vorakiat, C., Marconi, M. C., Menoni, C. S., Murnane, M. M., Rocca, J. J., Kapteyne, H. C., and Miao, J., "High numerical aperture tabletop soft x-ray diffraction microscope with 70-nm resolution", PNAS, 105(1), 24-27 (2008).

[9] Mills, B., Chau, C. F., Rogers, E. T. F., Grant-Jacob, J., Stebbings, S. L., Praeger, M., de Paula, A. M., Froud, C. A., Chapman, R. T., Butcher, T. J., Baumberg, J. J., Brocklesby, W. S., and Frey, J. G., "Direct measurement of the complex refractive index in the extreme ultraviolet spectral region using diffraction from a nanosphere array", Appl. Phys. Letters, 93, 231103 (2008).

[10] Svelto, O., [Principles of Lasers], Plenum Press, New York and London, 4th edition, ch.4 (1998).

[11] Stebbings, S. L., Rogers, E. T. F., de Paula, A. M., Praeger, M., Mills, B., Hanna, D. C., Baumberg, J. J., Brocklesby, W. S., and Frey, J. G., "Molecular variation of capillary-produced soft x-ray high harmonics", J. Phys. B, 41, 145602 (2008).

[12] Ersoy, O, K., [Fourier Optics and Imaging], WileyBlackwell, (2007).